Direct Observation of Corner States in Second-Order Topological Photonic Crystal Slabs

Xiao-Dong Chen,[†] Wei-Min Deng,[†] Fu-Long Shi,[†] Fu-Li Zhao, Min Chen, and Jian-Wen Dong[*]
School of Physics and State Key Laboratory of Optoelectronic Materials and Technologies, Sun Yat-sen University, Guangzhou 510275, China

(Received 19 December 2018; published 14 June 2019)

Recently, higher-order topological phases that do not obey the usual bulk-edge correspondence principle have been introduced in electronic insulators and brought into classical systems, featuring in-gap corner or hinge states. In this Letter, using near-field scanning measurements, we show the direct observation of corner states in second-order topological photonic crystal slabs consisting of periodic dielectric rods on a perfect electric conductor. Based on the generalized two-dimensional Su-Schrieffer-Heeger model, we show that the emergence of corner states roots in the nonzero edge dipolar polarization instead of the nonzero bulk quadrupole polarization. We demonstrate the topological transition of two-dimensional Zak phases of photonic crystal slabs by tuning intracell distances between two neighboring rods. We also directly observe in-gap one-dimensional edge states and zero-dimensional corner states in the microwave regime. Our work presents that the photonic crystal slab is a powerful platform to directly observe topological states and paves the way to study higher-order photonic topological insulators.

DOI: 10.1103/PhysRevLett.122.233902

Topological insulators host robust edge states predicted by the bulk-edge correspondence principle: A d-dimensional (dD) topological insulator with dD insulating bulk states supports $(d-1)$D conducting edge states [1–3]. This bulk-edge correspondence principle explains some topological properties, such as the soliton formation in polyacetylene based on the 1D Su-Schrieffer-Heeger model [4] and gapless edge states in 2D topological insulators [5,6]. Recently, higher-order topological insulators that do not obey the usual form of the bulk-edge correspondence principle have been introduced [7–24]. For example, a second-order 2D topological insulator has gapped 1D edge states but gapless 0D corner states. After the proposal in electronic insulators, higher-order topological phases have been realized in classical systems without the limitation imposed by the Fermi level. So far, 0D corner states have been observed in second-order insulators with the quantized bulk quadrupole polarization [15–17] or with the quantized edge dipolar polarization [12,20,21]. However, the latter kind of corner states have not been experimentally observed in photonic systems.

Photonic crystals (PCs) are periodic optical structures where many fancy photonic phenomena such as negative refraction [25], cloaking effect [26], and angular selectivity [27] were observed. With tunable geometric structures and controllable band dispersions, PCs were used to emulate topological behaviors. For example, researchers have observed the photonic analog of the quantum Hall, spin Hall, and valley Hall effect in PCs [28–37]. However, most reported 2D topological PCs require a metallic cover in experiments to prevent the radiation of electromagnetic waves into free space. This metallic cover not only complicates the experimental setup but also hampers the direct mapping of electromagnetic fields. In view of demands, a compact platform without the metallic cover is needed to realize the direct observation of topological states.

Here, we report the direct observation of corner states in second-order topological PC slabs consisting of dielectric rods on a perfect electric conductor. Our designed PC slab is free of the metallic cover, enabling the direct observation of topological states. Moreover, this structure can not only double the effective height of rods but also possess a full band gap, as compared with freestanding PC slabs. Based on the generalized 2D Su-Schrieffer-Heeger model, we show that the emergence of corner states is rooted in the nonzero edge dipolar polarization. We demonstrate the topological transition of 2D Zak phases by expanding or shrinking four dielectric rods in the unit cell. In-gap 1D edge states and 0D corner states are directly visualized.

We consider the freestanding square-lattice PC slab whose unit cell consists of four close-packed dielectric rods with the permittivity of $\varepsilon = 9.5$ in the air [Fig. 1(a)]. The in-plane lattice constant is $a = 25$ mm, and the height and diameter of the rods are $h = 50$ mm and $d = 5$ mm, respectively. Figure 1(c) shows its bulk band structures in which TM-like and TE-like bands are marked in blue and red, respectively. The TM-like band gap ranges from 4.55 to 5.34 GHz. However, the large height-diameter ratio ($h/d = 10$) increases the difficulty of sample fabrication. In addition, there is no full band gap if both TM-like and TE-like modes are considered. These two disadvantages can be overcome by considering a PC slab with rods on a perfect electric conductor [Fig. 1(b)]. First, the effective

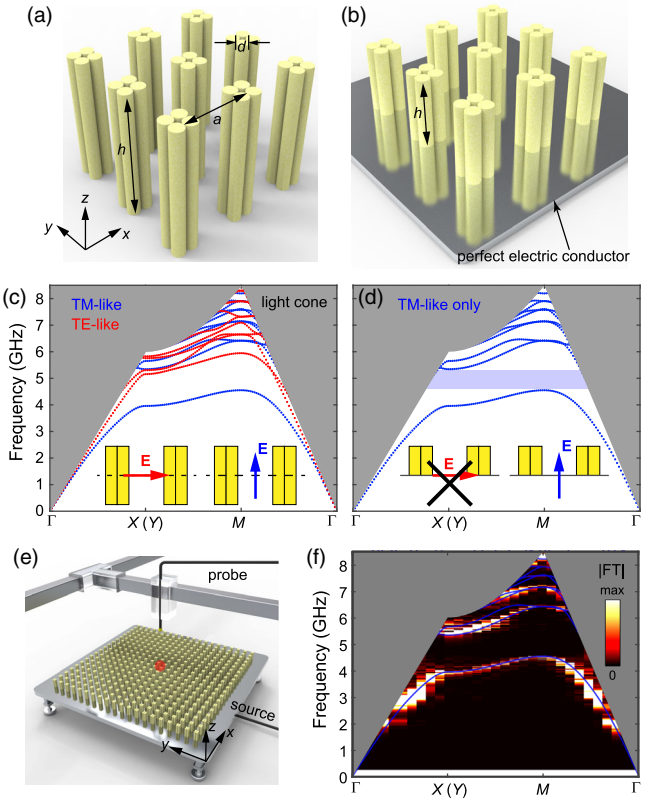

FIG. 1. (a) Schematics and (c) bulk band structures of the freestanding photonic crystal slab. The in-plane lattice constant is a, and the diameter and height of rods are d and h, respectively. Insets: In-plane and out-of-plane electric fields of TE-like and TM-like modes. TM-like and TE-like bands are marked in blue and red, respectively. The light cone is shaded in gray. (b) Schematic and (d) bulk band structures of the photonic crystal slab with rods standing on a perfect electric conductor. Insets: Only TM-like modes exist, as TE-like modes are filtered out. A full band gap is found (shaded in blue). (e) Setup for the near-field scanning measurement. (f) Measured (bright color) and calculated (blue line) bulk band structures.

height of the rods is double. To see this, we consider rods with $h = 25$ mm on a perfect electric conductor. Figure 1(d) shows its bulk band structures, which are exactly the same as TM-like bands in Fig. 1(c). It confirms that the effective height of the rods is double, because $h = 25$ mm in Fig. 1(b) while $h = 50$ mm in Fig. 1(a). Second, the perfect electric conductor requires that electric fields are perpendicular to the boundary, i.e., $E_x = E_y = 0$. Hence, TE-like modes are filtered out and TM-like modes are kept [inset in Fig. 1(d)]. Hence, a full band gap is found (shaded in blue). Note that, in numerical electromagnetics, the perfect electric conductor is applied to a boundary for TM modes of symmetric structures and halves the simulation space. To prove the theoretical proposal, we construct the sample in which periodic ceramic rods with $h = 25$ mm are put on a metallic plate [Fig. 1(e)]. This metallic plate behaves as a perfect electric conductor in the microwave regime. A source antenna is inserted through the drilled hole in the metallic substrate to excite eigenstates of the PC slabs. The signal is measured by a probe antenna, and measured E_z fields are collected by the vector network analyzer. By performing the Fourier transform on scanned E_z fields, we obtain measured bulk bands which are in good agreement with calculated bulk bands [Fig. 1(f)].

The above PC slab is the photonic realization of the 2D Su-Schrieffer-Heeger model, in which intracell distances between two neighboring rods are given by d_x and d_y [Fig. 2(a)]. By considering the first bulk band, the topology of the PC slab is given by the 2D Zak phase $\mathbf{Z} = (Z_x, Z_y)$:

$$Z_j = \int dk_x dk_y \mathrm{Tr}[\hat{A}_j(k_x, k_y)], \tag{1}$$

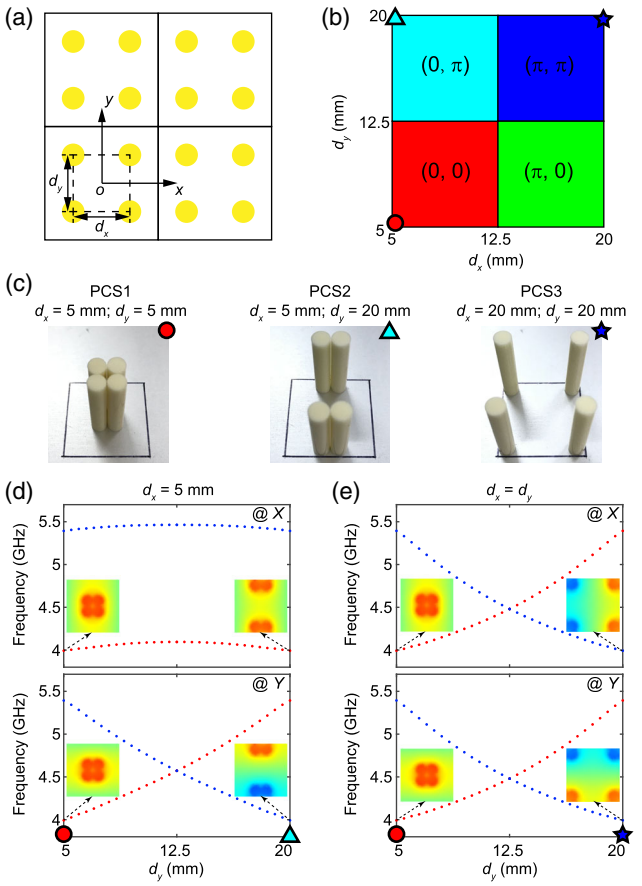

FIG. 2. (a) Schematic of the photonic crystal slab with four unit cells. Distances between the two rods are d_x and d_y. (b) Classification of photonic crystal slabs based on the 2D Zak phase $\mathbf{Z} = (Z_x, Z_y)$. Photonic crystal slabs are classified into four regions. Three representative photonic crystal slabs are labeled by the red circle, cyan triangle, and blue star. (c) Photos of three representative photonic crystal slabs with (left) $d_x = 5$ mm, $d_y = 5$ mm, (middle) $d_x = 5$ mm, $d_y = 20$ mm, and (right) $d_x = 20$ mm, $d_y = 20$ mm. (d),(e) Evolution of the two lowest bulk states along with d_y while (d) keeping $d_x = 5$ mm or (e) keeping $d_x = d_y$. Mirror symmetric (antisymmetric) states are marked in red (blue). Insets: E_z fields of the first lowest bulk states.

where $j = x$ or y and $\hat{A}_j(k_x, k_y) = i\langle u(\mathbf{k})|\partial_{k_j}|u(\mathbf{k})\rangle$ with $|u(\mathbf{k})\rangle$ the periodic Bloch function. The 2D Zak phase is related to the 2D bulk polarization via $Z_j = 2\pi P_j$ [24,38]. For PC slabs with mirror symmetry along the j direction, Z_j is quantized to 0 or π, and Z_j is related to the symmetry of Bloch modes at the zone center and boundary [39]. As the first bulk state at the Γ point is mirror symmetric, Z_x is 0 (π) when the bulk state at the X point is mirror symmetric (mirror antisymmetric). Z_y is determined by considering the bulk state at the Y point. Take the PC slab with $d_x =$ 5 mm and $d_y = 5$ mm as an example [left panel in Fig. 2(c)]. As the bulk state at the X (Y) point is mirror symmetric [left insets in Fig. 2(d)], Z_x (Z_y) is 0 (0). This PC slab (named PCS1) is characterized by $\mathbf{Z} = (0, 0)$. We can tune d_x or d_y to achieve topological phase transitions. Figure 2(d) plots the frequency spectra of the two lowest bulk states at the X and Y points by increasing d_y from 5 to 20 mm while keeping $d_x = 5$ mm. The mirror symmetric and antisymmetric states are labeled in red and blue, respectively. The lowest bulk state at the X point remains mirror symmetric, as there is no mode exchange. However, two bulk states at the Y point move closer, touch, and separate with the increasing of d_y. After the mode exchange at $d_y = 12.5$ mm, the PC slab is characterized by $Z_y = \pi$, as the lowest bulk state at the Y point becomes mirror antisymmetric. One representative PC slab with $d_x =$ 5 mm and $d_y = 20$ mm is shown in the middle panel in Fig. 2(c) and named PCS2. Similarly, PC slabs with $Z_x = \pi$ are obtained when $d_x > 12.5$ mm. Because both Z_x and Z_y are either 0 or π, PC slabs are classified into four different topological phases [Fig. 2(b)]. Particularly, we can obtain PC slabs with a nonzero Zak phase along both two directions, e.g., a PC slab with $d_x = 20$ mm and $d_y =$ 20 mm [right panel in Fig. 2(c) and named PCS3]. To see the phase transition from PCS1 to PCS3, we consider PC slabs with $d_x = d_y$. Figure 2(e) plots frequency spectra of the two lowest bulk states at the X and Y points. After the mode exchange at both k points, PC slabs are characterized by $\mathbf{Z} = (\pi, \pi)$, as the two bulk states become mirror antisymmetric [right insets in Fig. 2(e)].

The topological distinction between PC slabs with different Z_j guarantees the existence of edge states. As Z_y is 0 for PCS1, while it is π for PCS2 (or PCS3), there are edge states along the x direction for the boundary between PCS1 and PCS2 (or PCS3). To verify this, we first construct the boundary between PCS1 and PCS2 [Fig. 3(a)]. We put the source antenna at the left and scan E_z fields. Measured E_z fields of the edge state at $f = 4.47$ GHz are shown in Fig. 3(b), illustrating the confinement of fields at the interface. Measured E_z fields at more frequencies are given in Fig. S1 [40]. By performing the Fourier transform of measured E_z fields, the dispersion of edge states is shown by the bright color in Fig. 3(c). The measured edge dispersion agrees well with the simulated dispersion marked by the green line. Gapped edge states are confirmed, as the dispersion does not cover the whole bulk band gap. In addition, with measured E_z fields at the frequencies of 4.39 (at $k_x = 0$) and 5.18 GHz (at $k_x = \pi/a$), we retrieve eigenfields of edge states at the zone center and boundary [Fig. 3(c)]. Both edge states are mirror symmetric, indicating the zero edge dipolar polarization. To have a nonzero edge dipolar polarization, we

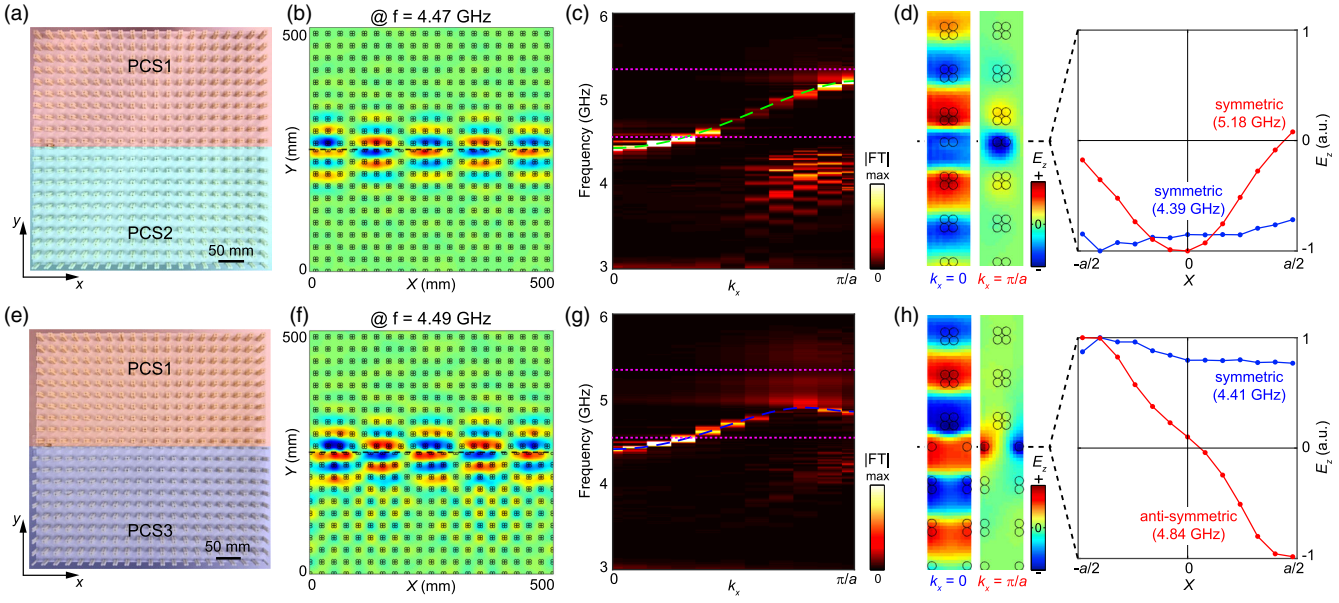

FIG. 3. (a) The boundary between PCS1 and PCS2. (b) Measured E_z fields of the edge state. (c) Measured (bright color) and calculated (green line) gapped edge band dispersions. Two pink dashed lines mark frequencies of the bulk band gap. (d) Retrieved E_z fields at the zone center and zone boundary. Both E_z fields are mirror symmetric. (e)–(h) Measured results for the boundary between PCS1 and PCS3. The edge state at the zone center is mirror symmetric, while that at the zone boundary is mirror antisymmetric.

consider the boundary between PCS1 and PCS3 [Fig. 3(e)]. We also scan E_z fields (see Fig. S2 [40]) and obtain the measured edge dispersion, which is in good agreement with the calculated dispersion [Fig. 3(g)]. Gapped edge states are found, but their dispersion curve is different to that in Fig. 3(c), indicating that they have different features. To see this, we retrieve eigenfields of edge states at the frequencies of 4.41 (at $k_x = 0$) and 4.84 GHz (at $k_x = \pi/a$) [Fig. 3(h)]. The edge state at the zone center is mirror symmetric, while that at the zone boundary is mirror antisymmetric. It confirms the nonzero edge dipolar polarization.

The nonzero edge dipolar polarization between PCS1 and PCS3 indicates the existence of corner states. Hence, we construct the experimental sample for observing corner states [Fig. 4(a)]. It consists of PCS3 at the center while PCS1 is at the background. In the experiment, we put a source antenna near the top-right corner. Figure 4(b) shows measured E_z fields at one example frequency of 4.01 GHz (see more E_z fields at more frequencies in Fig. S3 [40]). To identify bulk, edge, and corner states, we apply three binary filters [lower panel in Fig. 4(b)] to separate responses of different eigenstates. Note that key features of measured results are visible without the application of filters, and these binary filters are used to have a better demonstration (see the discussion in Supplemental Material, Sec. C [40].

Figure 4(c) shows the resulting spectra, in which high values indicate the existence of eigenstates and zero (or low) values mean the presence of band gaps. Within the bulk and edge gaps, a resonance of the corner spectrum is found near 5.2 GHz. It corresponds to the corner state whose existence is predicted according to the nonzero edge dipolar polarization [Fig. 4(d)]. The enlarged E_z fields clearly demonstrate that fields of the corner state are confined around the top-right single rod [left panel in Fig. 4(e)]. Note that corner states still survive when the rotational symmetry of the sample is reduced to C_2 symmetry [41]. The field confinement is also achieved when the source frequency is beyond that of corner states, e.g., $f = 4.98$ GHz [right panel in Fig. 4(e)]. But these two kinds of field confinement are different, because corner states are immune to the source position while the other is dependent on the source position. Lastly, we carry out a comparative sample without corner states [Fig. 4(f)]. Within the bulk and edge gaps, there is no resonance of corner spectra. It proves the absence of corner states due to the zero edge dipolar polarization between PCS1 and PCS2. More discussion including the presence (absence) of edge states at the top (right) boundary is given in Fig. S4 [40].

In conclusion, we design and demonstrate PC slabs with periodic dielectric rods on a perfect electric conductor.

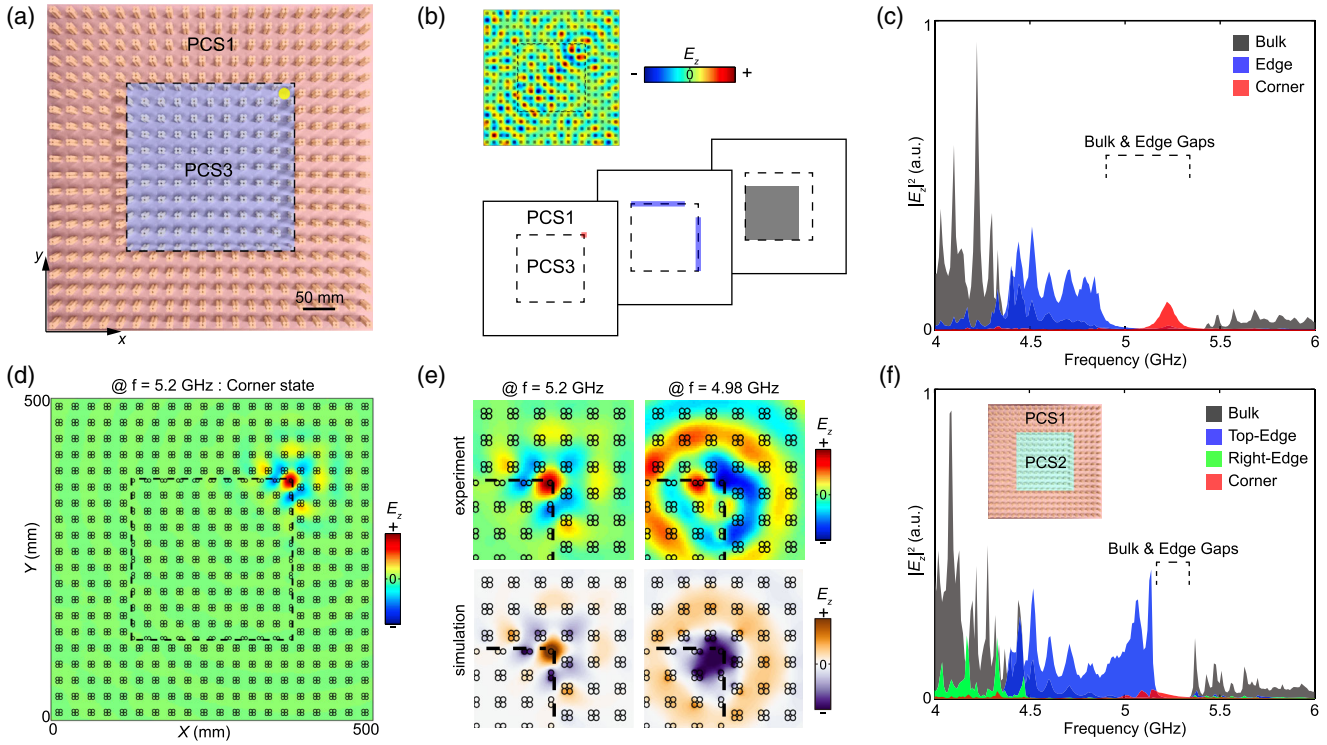

FIG. 4. (a) The sample for measuring corner states. The black dashed square indicates boundaries between PCS1 and PCS3. The yellow dot marks the position of the source antenna. (b) The response of the sample at 4.01 GHz. Measured $|E_z|^2$ are multiplied by three binary filters to determine bulk (gray), edge (blue), and corner (red) responses. (c) Spectra of bulk, edge, and corner states, showing different resonant frequencies. (d) Measured E_z fields of the corner state at 5.2 GHz. (e) Measured and simulated E_z fields at 5.2 and 4.98 GHz. Different color bars are used for measured and simulated results. (f) Bulk, edge, and corner spectra of the sample (between PCS1 and PCS2) without corner states.

Based on the 2D Su-Schrieffer-Heeger model, we illustrate the topological phase map of 2D Zak phases and the topological phase transition. Inherent from the nonzero Zak phase of bulk states, we directly observe corner states induced by the nonzero edge dipolar polarization. This is the key identifying feature of second-order topological PC slabs in which 0D corner states are predicted by the nontrivial Zak phase of 2D bulk states. Our results demonstrate that second-order photonic topological insulators can guide the light flow and trap the light. Although the metal ground plane becomes lossy at optical frequencies, alternative designs such as a square array of silicon nanopillars [42] or interconnected veins [43] can be employed.

Corner states in topological PC slabs have potential applications in enhancing light-matter interaction. For example, corner states can serve as high-Q cavity modes, which are exploited to enhance optical nonlinear effect and optical sensing [44,45]. Another attractive property is the coexistence of corner and edge states, which may enable the integration of the microcavity laser and the waveguide on a single chip [46,47]. The Su-Schrieffer-Heeger model, which is proposed in solid-state physics, is generalized to photonic systems with adjustable hopping strength. The topological phase map and corner states are extendable to other bosonic systems such as acoustic systems.

This work was supported by National Natural Science Foundation of China (Grants No. 11704422, No. 11761161002, and No. 61775243), Natural Science Foundation of Guangdong Province (Grant No. 2018B030308005), and Science and Technology Program of Guangzhou (Grant No. 201804020029).

Note added.—We found independent discoveries of corner states and higher-order topological states in other photonic systems [48–52].

*Corresponding author.
dongjwen@mail.sysu.edu.cn
†X.-D. C., W.-M. D., and F.-L. S. contributed equally to this work.

[1] X.-L. Qi and S.-C. Zhang, Topological insulators and superconductors, Rev. Mod. Phys. **83**, 1057 (2011).
[2] D. Xiao, M.-C. Chang, and Q. Niu, Berry phase effects on electronic properties, Rev. Mod. Phys. **82**, 1959 (2010).
[3] M. Z. Hasan and C. L. Kane, Colloquium: Topological insulators, Rev. Mod. Phys. **82**, 3045 (2010).
[4] W. P. Su, J. R. Schrieffer, and A. J. Heeger, Solitons in Polyacetylene, Phys. Rev. Lett. **42**, 1698 (1979).
[5] C. L. Kane and E. J. Mele, Z2 Topological Order and the Quantum Spin Hall Effect, Phys. Rev. Lett. **95**, 146802 (2005).
[6] H. C. Manoharan, Topological insulators: A romance with many dimensions, Nat. Nanotechnol. **5**, 477 (2010).
[7] W. A. Benalcazar, B. A. Bernevig, and T. L. Hughes, Electric multipole moments, topological multipole moment pumping, and chiral hinge states in crystalline insulators, Phys. Rev. B **96**, 245115 (2017).
[8] W. A. Benalcazar, B. A. Bernevig, and T. L. Hughes, Quantized electric multipole insulators, Science **357**, 61 (2017).
[9] J. Langbehn, Y. Peng, L. Trifunovic, F. von Oppen, and P. W. Brouwer, Reflection-Symmetric Second-Order Topological Insulators and Superconductors, Phys. Rev. Lett. **119**, 246401 (2017).
[10] Z. Song, Z. Fang, and C. Fang, (d–2)-Dimensional Edge States of Rotation Symmetry Protected Topological States, Phys. Rev. Lett. **119**, 246402 (2017).
[11] F. Schindler, A. M. Cook, M. G. Vergniory, Z. Wang, S. S. P. Parkin, B. A. Bernevig, and T. Neupert, Higher-order topological insulators, Sci. Adv. **4**, eaat0346 (2018).
[12] M. Ezawa, Higher-Order Topological Insulators and Semimetals on the Breathing Kagome and Pyrochlore Lattices, Phys. Rev. Lett. **120**, 026801 (2018).
[13] M. Geier, L. Trifunovic, M. Hoskam, and P. W. Brouwer, Second-order topological insulators and superconductors with an order-two crystalline symmetry, Phys. Rev. B **97**, 205135 (2018).
[14] F. K. Kunst, G. van Miert, and E. J. Bergholtz, Lattice models with exactly solvable topological hinge and corner states, Phys. Rev. B **97**, 241405(R) (2018).
[15] M. Serra-Garcia, V. Peri, R. Susstrunk, O. R. Bilal, T. Larsen, L. G. Villanueva, and S. D. Huber, Observation of a phononic quadrupole topological insulator, Nature (London) **555**, 342 (2018).
[16] C. W. Peterson, W. A. Benalcazar, T. L. Hughes, and G. Bahl, A quantized microwave quadrupole insulator with topologically protected corner states, Nature (London) **555**, 346 (2018).
[17] S. Imhof, C. Berger, F. Bayer, J. Brehm, L. W. Molenkamp, T. Kiessling, F. Schindler, C. H. Lee, M. Greiter, T. Neupert, and R. Thomale, Topolectrical-circuit realization of topological corner modes, Nat. Phys. **14**, 925 (2018).
[18] J. Noh, W. A. Benalcazar, S. Huang, M. J. Collins, K. P. Chen, T. L. Hughes, and M. C. Rechtsman, Topological protection of photonic mid-gap defect modes, Nat. Photonics **12**, 408 (2018).
[19] F.-F. Li, H.-X. Wang, Z. Xiong, Q. Lou, P. Chen, R.-X. Wu, Y. Poo, J.-H. Jiang, and S. John, Topological light-trapping on a dislocation, Nat. Commun. **9**, 2462 (2018).
[20] H. Xue, Y. Yang, F. Gao, Y. Chong, and B. Zhang, Acoustic higher-order topological insulator on a kagome lattice, Nat. Mater. **18**, 108 (2019).
[21] X. Ni, M. Weiner, A. Alù, and A. B. Khanikaev, Observation of higher-order topological acoustic states protected by generalized chiral symmetry, Nat. Mater. **18**, 113 (2019).
[22] X. Zhang, H.-X. Wang, Z.-K. Lin, Y. Tian, B. Xie, M.-H. Lu, Y.-F. Chen, and J.-H. Jiang, Second-order topology and multidimensional topological transitions in sonic crystals, Nat. Phys. **15**, 582 (2019).
[23] X. Zhang, Z.-K. Lin, H.-X. Wang, Y. Tian, M.-H. Lu, Y.-F. Chen, and J.-H. Jiang, Acoustic hierarchical topological insulators, arXiv:1811.05514.
[24] B.-Y. Xie, H.-F. Wang, H.-X. Wang, X.-Y. Zhu, J.-H. Jiang, M.-H. Lu, and Y.-F. Chen, Second-order photonic topological insulator with corner states, Phys. Rev. B **98**, 205147 (2018).

[25] E. Cubukcu, K. Aydin, E. Ozbay, S. Foteinopoulou, and C. M. Soukoulis, Negative refraction by photonic crystals, Nature (London) **423**, 604 (2003).
[26] X. Huang, Y. Lai, Z. H. Hang, H. Zheng, and C. T. Chan, Dirac cones induced by accidental degeneracy in photonic crystals and zero-refractive-index materials, Nat. Mater. **10**, 582 (2011).
[27] Y. Shen, D. Ye, I. Celanovic, S. G. Johnson, J. D. Joannopoulos, and M. Soljačić, Optical broadband angular selectivity, Science **343**, 1499 (2014).
[28] Z. Wang, Y. Chong, J. D. Joannopoulos, and M. Soljačić, Observation of unidirectional backscattering-immune topological electromagnetic states, Nature (London) **461**, 772 (2009).
[29] Y. Poo, R.-x. Wu, Z. Lin, Y. Yang, and C. T. Chan, Experimental Realization of Self-Guiding Unidirectional Electromagnetic Edge States, Phys. Rev. Lett. **106**, 093903 (2011).
[30] A. B. Khanikaev, S. H. Mousavi, W.-K. Tse, M. Kargarian, A. H. MacDonald, and G. Shvets, Photonic topological insulators, Nat. Mater. **12**, 233 (2013).
[31] W.-J. Chen, S.-J. Jiang, X.-D. Chen, B. Zhu, L. Zhou, J.-W. Dong, and C. T. Chan, Experimental realization of photonic topological insulator in a uniaxial metacrystal waveguide, Nat. Commun. **5**, 5782 (2014).
[32] L.-H. Wu and X. Hu, Scheme for Achieving a Topological Photonic Crystal by Using Dielectric Material, Phys. Rev. Lett. **114**, 223901 (2015).
[33] Y. Yang, Y. F. Xu, T. Xu, H.-X. Wang, J.-H. Jiang, X. Hu, and Z. H. Hang, Visualization of a Unidirectional Electromagnetic Waveguide Using Topological Photonic Crystals Made of Dielectric Materials, Phys. Rev. Lett. **120**, 217401 (2018).
[34] S. Barik, A. Karasahin, C. Flower, T. Cai, H. Miyake, W. DeGottardi, M. Hafezi, and E. Waks, A topological quantum optics interface, Science **359**, 666 (2018).
[35] T. Ma and G. Shvets, All-Si valley-Hall photonic topological insulator, New J. Phys. **18**, 025012 (2016).
[36] J.-W. Dong, X.-D. Chen, H. Zhu, Y. Wang, and X. Zhang, Valley photonic crystals for control of spin and topology, Nat. Mater. **16**, 298 (2017).
[37] X.-D. Chen, F.-L. Zhao, M. Chen, and J.-W. Dong, Valley-contrasting physics in all-dielectric photonic crystals: Orbital angular momentum and topological propagation, Phys. Rev. B **96**, 020202(R) (2017).
[38] F. Liu and K. Wakabayashi, Novel Topological Phase with a Zero Berry Curvature, Phys. Rev. Lett. **118**, 076803 (2017).
[39] M. Xiao, Z. Q. Zhang, and C. T. Chan, Surface Impedance and Bulk Band Geometric Phases in One-Dimensional Systems, Phys. Rev. X **4**, 021017 (2014).
[40] See Supplemental Material at http://link.aps.org/supplemental/10.1103/PhysRevLett.122.233902 for sections (A) measured E_z fields of gapped edge states of two boundaries, (B) measured E_z fields of samples with and without corner states, (C) binary filters, (D) robustness of corner states, (E) system shape and features of edge or corner states, (F) difference between two kinds of field confinement.
[41] W. A. Benalcazar, T. Li, and T. L. Hughes, Quantization of fractional corner charge in C_n-symmetric higher-order topological crystalline insulators, arXiv:1809.02142.
[42] X.-T. He, Z.-Z. Huang, M.-L. Chang, S.-Z. Xu, F.-L. Zhao, S.-Z. Deng, J.-C. She, and J.-W. Dong, Realization of zero-refractive-index lens with ultralow spherical aberration, ACS Photonics **3**, 2262 (2016).
[43] J. D. Joannopoulos, S. G. Johnson, J. N. Winn, and R. D. Meade, *Photonic Crystals—Molding the Flow of Light* (Princeton University Press, Princeton, NJ, 2008).
[44] J. Bravo-Abad, A. Rodriguez, P. Bermel, S. G. Johnson, J. D. Joannopoulos, and M. Soljačić, Enhanced nonlinear optics in photonic-crystal microcavities, Opt. Express **15**, 16161 (2007).
[45] A. Di Falco, L. O'Faolain, and T. F. Krauss, Chemical sensing in slotted photonic crystal heterostructure cavities, Appl. Phys. Lett. **94**, 063503 (2009).
[46] M. Yoshida, M. De Zoysa, K. Ishizaki, Y. Tanaka, M. Kawasaki, R. Hatsuda, B. Song, J. Gelleta, and S. Noda, Double-lattice photonic-crystal resonators enabling high-brightness semiconductor lasers with symmetric narrow-divergence beams, Nat. Mater. **18**, 121 (2019).
[47] F. Alpeggiani and L. Kuipers, Topological edge states in bichromatic photonic crystals, Optica **6**, 96 (2019).
[48] B.-Y. Xie, G.-X. Su, H.-F. Wang, H. Su, X.-P. Shen, P. Zhan, M.-H. Lu, Z.-L. Wang, and Y.-F. Chen, following Letter, Visualization of Higher-Order Topological Insulating Phases in Two-Dimensional Dielectric Photonic Crystals, Phys. Rev. Lett. **122**, 233903 (2019).
[49] A. E. Hassan, F. K. Kunst, A. Moritz, G. Andler, E. J. Bergholtz, and M. Bourennane, Corner states of light in photonic waveguides, arXiv:1812.08185.
[50] S. Mittal, V. V. Orre, G. Zhu, M. A. Gorlach, A. Poddubny, and M. Hafezi, Photonic quadrupole topological phases, arXiv:1812.09304.
[51] Y. Ota, F. Liu, R. Katsumi, K. Watanabe, K. Wakabayashi, Y. Arakawa, and S. Iwamoto, Photonic crystal nanocavity based on a topological corner state, arXiv:1812.10171.
[52] L. Zhang, Y. Yang, P. Qin, Q. Chen, F. Gao, E. Li, J.-H. Jiang, B. Zhang, and H. Chen, Higher-order photonic topological states in surface-wave photonic crystals, arXiv:1901.07154.